THE JOURNAL OF BIOLOGICAL CHEMISTRY VOL. 284, NO. 38, pp. 25512–25521, September 18, 2009

Intrinsic Voltage Dependence of the Epithelial Na^+ Channel Is Masked by a Conserved Transmembrane Domain Tryptophan*[S]

Received for publication, May 1, 2009, and in revised form, June 19, 2009 Published, JBC Papers in Press, July 20, 2009, DOI 10.1074/jbc.M109.015917

Oleh Pochynyuk[‡], Volodymyr Kucher[‡], Nina Boiko[‡], Elena Mironova[‡], Alexander Staruschenko[§], Alexey V. Karpushev[§], Qiusheng Tong[‡], Eunan Hendron[‡], and James Stockand[‡1]

From the [‡]Department of Physiology, University of Texas Health Science Center, San Antonio, Texas 78229 and the [§]Department of Physiology, Kidney Disease Center, Medical College of Wisconsin, Milwaukee, Wisconsin 53226

Tryptophan residues critical to function are frequently located at the lipid-water interface of transmembrane domains. All members of the epithelial Na^+ channel (ENaC)/Degenerin (Deg) channel superfamily contain an absolutely conserved Trp at the base of their first transmembrane domain. Here, we test the importance of this conserved Trp to ENaC/Deg function. Targeted substitution of this Trp in mouse ENaC and rat ASIC subunits decrease channel activity. Differential substitution with distinct amino acids in α-mENaC shows that it is loss of this critical Trp rather than introduction of residues having novel properties that changes channel activity. Surprisingly, Trp substitution unmasks voltage sensitivity. Mutant ENaC has increased steady-state activity at hyperpolarizing compared with depolarizing potentials associated with transient activation and deactivation times, respectively. The times of activation and deactivation change 1 ms/mV in a linear manner with rising and decreasing slopes, respectively. Increases in macroscopic currents at hyperpolarizing potentials results from a voltage-dependent increase in open probability. Voltage sensitivity is not influenced by divalent cations; however, it is Na^+-dependent with a 63-mV decrease in voltage required to reach half-maximal activity per log increase in $[Na^+]$. Mutant channels are particularly sensitive to intracellular $[Na^+]$ for removing this sodium abolishes voltage dependence. We conclude that the conserved Trp at the base of TM1 in ENaC/Deg channels protects against voltage by masking an inhibitory allosteric or pore block mechanism, which decreases activity in response to intracellular Na^+.

Proteins encoded by the epithelial Na^+ channel (ENaC)[2]/Degenerin (Deg) gene superfamily comprise an ion channel family found in all metazoan animals ranging from *Hydra* and *Caenorhabditis elegans* to the common garden snail, fly, and man (1–3). Members of this important ion channel family serve diverse functions and have a wide tissue distribution, including being in epithelial and neuronal tissues. Phenotypes resulting from ENaD/Deg gain and loss of function highlight the physiological importance of these ion channels. In *C. elegans*, diminished function of degenerins disrupts proprioception and mechanosensation; whereas, gain of function leads to neuronal degeneration (3). In mammals, including man, loss of ENaC function causes renal salt wasting and excessively wet airways; whereas, gain of function causes dry airways, and inappropriate renal salt conservation leading to hypertension (4, 5).

Jasti *et al.* (6) recently made a seminal contribution to understanding ENaC/Deg channels by providing a crystal structure with atomic level resolution for most of the homomeric chicken ASIC1 channel. This channel was in a pseudo-inactive state possibly resembling a closed channel conformation. The cASIC1 crystal structure confirmed that ENaC/Deg channels are trimeric (6, 7). Some family members, as typified by ASIC, form homotrimeric and heterotrimeric channels. Others, such as ENaC, are obligatory heterotrimers (1–3, 8). All ENaC/Deg subunits are thought to share a common tertiary structure having intracellular, cytosolic NH_2 and COOH tails separated from a large extracellular domain by two transmembrane-spanning domains: transmembrane domain 1 (TM1) and 2 (TM2) (1, 2, 6, 9).

ENaC/Deg channels are Na^+-selective, not overtly sensitive to voltage having no time-dependent activation or inactivation and have linear current-voltage relations at the single channel level with relatively low unitary conductances ranging between 4 and 10 pS (1, 2). Moreover, a hallmark of these channels, particularly ENaC, is slow gating kinetics with open and closed times in the range of seconds.

The ENaC/Deg pore is defined primarily by the linear TM2 helices of the three constituent subunits and does not involve P-loops as do the pores of K^+ channels (6, 10–12). The selectivity filter, also attributable to residues in TM2, is approximately half between the extracellular and intracellular mouths of the pore. The selectivity filter forms the narrowest part of the pore, which can be represented as two funnels closing toward the middle of the membrane (6). At the extracellular mouth of the pore, TM1 juxtaposes TM2 being a little outside the circumference of the pore as defined by TM2. At the intracellular mouth, TM1 and TM2 lie along the same circumference and are solvent-accessible, suggesting both transmembrane do-

* This work was supported, in whole or in part, by National Institutes of Health Grant R01DK70571 and AHA Grants 0640054N (to J. D. S.) and 0730111N. This work was also supported by a Carl W. Gottschalk Research Scholar Grant (American Society of Nephrology) (to A. S.) and 0825062F (American Heart Association) (to O. P.).

[S] The on-line version of this article (available at http://www.jbc.org) contains supplemental Table S1 and Figs. S1 and S2.

[1] To whom correspondence should be addressed: University of Texas Health Science Center, 7703 Floyd Curl Dr., San Antonio TX 78229-3900. Tel.: 210-567-4332; Fax: 210-567-4410; E-mail: stockand@uthscsa.edu.

[2] The abbreviations used are: ENaC, epithelial Na^+ channel; TM, transmembrane domain; HA, hemagglutinin; Deg, degenerin; gA, gramicidin A; GFP, green fluorescent protein; ASIC, acid-sensing ion channel.

mains contribute to the intracellular vestibule of the pore (6, 13–15). The actual gate of ENaC/Deg channels remains elusive but may be near the intracellular mouth of the pore (15).

Every ENaC/Deg protein contains a conserved tryptophan residue at the intracellular base of TM1: these Trp residues reside at the first cytosolic-plasma membrane interface of all ENaC/Deg polypeptides. Little is known about the possible importance of the conserved Trp in ENaC/Deg channels. One study finds that mutation of the Trp in TM1 of α-mENaC reduces activity (13). Mutation of the same Trp in human ASIC1a and snail FaNaC results in nonfunctional channels (14, 15).

A re-occurring feature common to many intrinsic membrane proteins, including ion channels, is that critical Trp residues often reside at lipid-water interfaces in helical transmembrane domains (16–21). Here they insert into the lipid membrane acting either as interfacial anchoring points setting the tilt of the transmembrane domain as it spans the membrane or hinge points providing allosteric linkage for gating.

We hypothesize that the conserved transmembrane domain Trp in ENaC/Deg channels serves a critical role with respect to channel function. To better understand the importance of this Trp, we quantified the effects of substituting it in mENaC. Targeted substitution of the critical Trp in α- and β-mENaC decreased channel activity and unmasked marked voltage sensitivity. Voltage sensitivity reflected voltage-dependent changes in open probability. Voltage sensitivity was Na^+-dependent with intracellular $[Na^+]$ playing a particularly important role in setting the voltage at which mutant ENaC had half-maximal activity. We conclude that stabilization of the pore by Trp at the base of TM1 lessens Na^+-dependent modulation of wild-type channels likely by interfering with an intrinsic allosteric or pore block mechanism. This is the first description of a mutation in ENaC/Deg channels that results in voltage sensitivity.

EXPERIMENTAL PROCEDURES

Chemicals and cDNA Constructs—All chemicals were from Sigma unless noted otherwise. All materials used in Western blot analysis were from Bio-Rad. Sulfo-NHS-LC-biotin and streptavidin-agarose were from Pierce. The mouse monoclonal anti-Myc antibody was from Clontech (Palo Atlo, CA). Anti-mouse horseradish peroxidase-conjugated secondary antibody was from Kirkegaard-Perry Laboratories (Gaithersburg, MD). ECL reagents were from PerkinElmer Life Sciences (Boston, MA). Expression vectors encoding rat ASIC1a, ASIC2b, and ASIC3 were a kind gift from Dr. P. K. Ahring and have been described previously (22, 23). The mammalian expression vectors encoding α-, β- and γ-mouse ENaC with NH_2-terminal Myc- and HA-epitope tags have been described previously (24–26). As noted in these earlier publications, channels comprised of epitope-tagged subunits have indistinguishable function from those lacking tags. All ENaC mutagenesis was performed on the backbone of plasmids encoding Myc-tagged subunits. Mutants created in our laboratory with QuikChange (Stratagene) mutagenesis per the manufacturer's instructions or outsourced to TOP Gene Technologies (Montreal, Canada). Regardless of source, every plasmid encoding mutant channel subunits was sequenced to ensure proper incorporation of the expected mutation and to confirm sequence identity, orientation and reading frame.

Cells and Expression of Recombinant Protein—Chinese Hamster Ovary cells were from American Type Culture Collection. These cells were maintained with standard culture conditions (Dulbecco's modified Eagle's medium + 10% fetal bovine serum, 37 °C, 5% CO_2) as described previously (24–26). Recombinant mENaC and rASIC were overexpressed in CHO cells by transfecting the appropriate expression plasmids using the Polyfect reagent (Qiagen, Valencia, CA) as described previously (24–26). Electrophysiological experiments were performed 48–72 h after transfection. For electrophysiology studies, 0.3 μg/subunit/9.6 cm^2 plasmid cDNA was used. For membrane-labeling studies, 1.0 μg/subunit/78.5 cm^2 plasmid cDNA was used.

Membrane Labeling Experiments—Membrane labeling experiments closely followed those described previously (25, 27, 28). In brief, CHO cells were transfected with Myc- and HA-tagged ENaC subunits. The subunit of interest contained the Myc tag and was followed with anti-Myc antibody. Forty-eight hours after transfection, cells were washed three times with ice-cold phosphate-buffered saline (PBS) (pH 8.0) and subsequently incubated with 3 mM sulfo-NHS-LC-biotin (in PBS, pH 8.0) for 30 min at room temperature in the dark. Cells were washed again three times with ice-cold PBS plus 100 mM glycine to quench the reaction and then, extracted in gentle lysis buffer (76 mM NaCl, 50 mM HCl-Tris, pH 7.4, 2 mM EGTA, plus 1% Nonidet P-40 and 10% glycerol; supplemented with the protease inhibitor, 1 mM phenylmethylsulfonyl fluoride). Extracts were cleared and normalized for total protein concentration. Pre-equilibrated streptavidin-agarose beads were agitated overnight at 4 °C with 400 μg of total protein. Agarose beads were then washed six times with gentle lysis buffer and subsequently resuspended in SDS sample buffer and 20 mM dithiothreitol, heated at 85 °C for 10 min, run on 7.5% polyacrylamide gels in the presence of SDS, transferred to nitrocellulose and probed with anti-Myc antibody in Tris-buffered saline supplemented with 5% dried milk and 0.1% Tween-20. Band intensity in developed blots was quantified by scanning the blots and then using SigmaGel (Jandel Scientific) to analyze digital images. We used a flood-above-threshold protocol with threshold set to the highest practical level.

Electrophysiology—Whole cell macroscopic current recordings of ENaC and ASIC reconstituted in CHO cells were made under voltage clamp conditions using standard methods (24–26). Current recordings were acquired with an Axopatch 200B (Axon Instr., Union City, CA) interfaced via a Digidata 1322A (Axon Instr.) to a PC running the pClamp 9.2 suite of software (Axon Instr.). All currents were filtered at 1 kHz. Whole cell capacitance was routinely compensated and was approximately ~9 pF for CHO cells. Series resistances, on average 2–5 MΩ, were also compensated. Only recordings where access resistance and capacitance changed less than 10% over the course of the experiment were used. Currents were evoked with standard voltage ramp and voltage step protocols. The specific protocols used in each experiment are described in "Results." (For experiments on ASIC, currents were evoked by rapid exchange of the

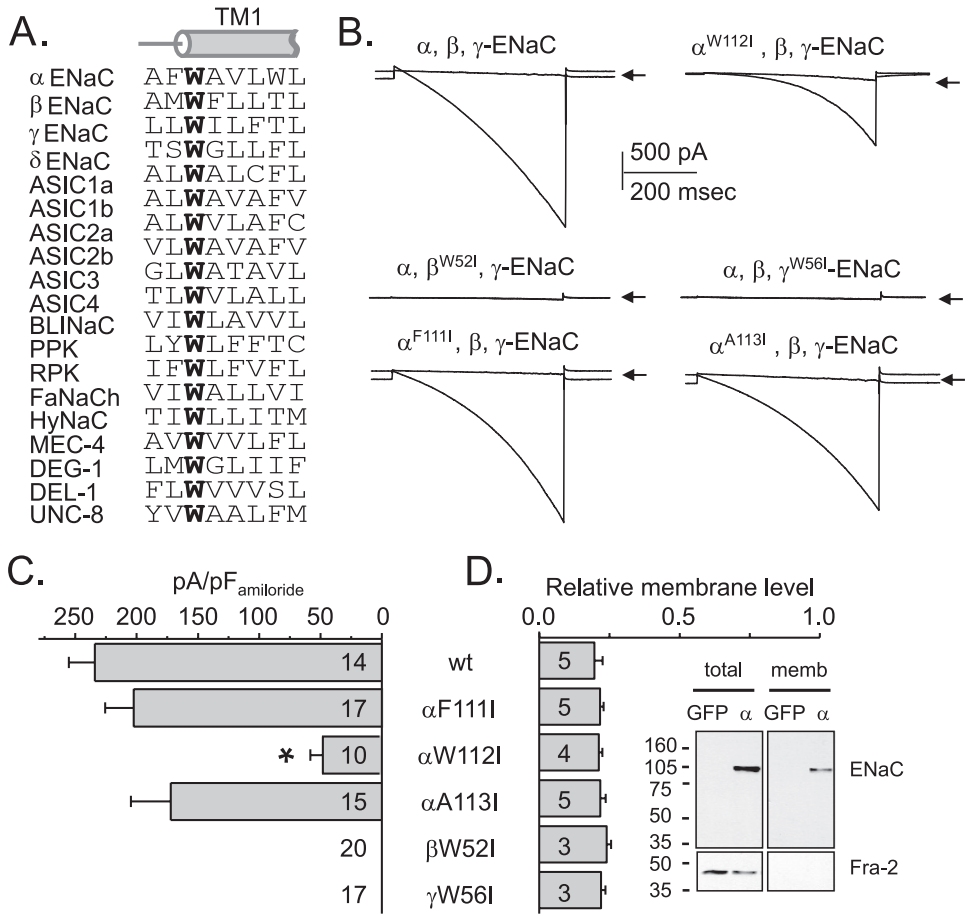

FIGURE 1. **Substitution of a critical Trp at the base of TM1 decreases ENaC activity but not membrane expression.** *A*, sequence alignment of the residues spanning the cytosolic-membrane interface for TM1 in ENaC/Deg channels. The subunit type is noted to the *left*. The position of the transmembrane domain is noted at the *top*. *B*, representative macroscopic currents before and after addition of amiloride (noted by *arrow*) for voltage-clamped CHO cells expressing wild-type and mutant ENaC containing one subunit with substituted Trp. Also shown are representative currents for channels containing α-subunits with the residues just before and after Trp substitution. Inward current is downwards. *C*, summary graph of activity reported as amiloride-sensitive current density for wild-type and mutant ENaC expressed in CHO cells. *, significant decrease compared with wild-type. *D*, summary graph of the relative membrane levels (to total expression levels) of wild-type and mutant ENaC. For each mutant, the subunit of interest was identified using an engineered Myc tag. Wild-type α-ENaC (having a Myc tag) was followed in the wild-type control group. The *inset* shows a typical experiment: the *top* Western blots were probed with anti-Myc antibody and contained the total cellular and membrane pool of proteins from control CHO cells expressing only GFP and cells expressing Myc-tagged α-mENaC with untagged β- and γ-mENaC. Membrane fractions isolated from 4× the amount of total cellular lysate loaded. As shown in the *lower panel*, these blots were stripped and counterprobed with anti-Fra-2, which is a cytosolic protein, to confirm good separation of the membrane fraction from total cellular pools. Molecular weights are noted to the *left*.

standard bathing solution for one with acidic pH 5.0.) Current data were collected in standard salt solutions as detailed under supplemental Table S1.

For symmetrical solutions, macroscopic current voltage (I-V) curves were normalized to instantaneous current at −100 mV. I-V curves in asymetrical solutions (150/5 *versus* 5/150) were normalized to instantaneous current 100 mV hyperpolarized from the reversal potential. Conductance-voltage (G-V) relations plotted as relative steady-state conductance (G/G_{max}) as a function of test potential. Data were fitted with the Boltzmann function ($G = G_{max}\{1/[1 + e^{-(V-V_{1/2})zF/RT}]\}$ normalizing to the maximum of the fit. Activation and deactivation time constants (τ) were obtained by fitting current traces to a single exponential function, $I = I_o e^{(-t/\tau)}$.

For excised, outside-out patches made on CHO cells overexpressing wild-type and mutant ENaC, current recordings were made under voltage-clamp conditions using an Axopatch 200B. Currents were low-pass filtered at 100 Hz by an eight-pole Bessel filter (Warner Instr.) digitized at 500 Hz, and stored on a PC using the Digidata 1322A interface. For presentation, some currents were subsequently software-filtered at 40 Hz. Gap-free current recordings were made at pipette potentials (V_p) ranging from 100 to −100 mV with inward current downwards. Current data were analyzed using pClamp 9.2. Channel activity defined as NP_o was equal to $\Sigma(t_1 + 2t_2 + ...it_i)$, where t_i is the fractional open time spent at each of the observed current levels. P_o was determined by dividing NP_o for the observed number of channels within a patch as established with all-point histograms. P_o calculated over ~30–120 s for each data point. Only patches containing five or fewer channels were used for analysis. Single channel current-voltage (*i*-V) relations were generated from unitary currents (*i*) defined by all-point histograms at different holding potentials from, at least, four independent experiments.

Statistics—All summarized data are reported as mean ± S.E. Membrane levels of ENaC were normalized to total cellular pools. Summarized data are compared with either the Student's *t* test or a one way analysis of variance in conjunction with the Dunnett post-test where appropriate. $p \leq 0.05$ is considered significant.

RESULTS

A Conserved Trp at the Base of TM1 Is Critical to ENaC/Deg Activity—As shown by the sequence alignment in Fig. 1*A*, an absolutely conserved tryptophan is located at the first intracellular membrane interface of all ENaC/Deg subunits. To begin probing the importance of this conserved residue to channel function, we created mutant mouse ENaC subunits containing isoleucine substitutions of these tryptophans (αW112I, βW52I, γW56I). In addition, we created mutants containing isoleucine substitutions of the residues just preceding and following the conserved Trp in α-mENaC (αF111I, αA113I). Fig. 1*B* shows representative macroscopic current traces from voltage-

clamped CHO cells expressing all wild-type (α-, β-, and γ-mENaC) subunits and channels containing one mutant subunit. Currents were evoked with a voltage ramp (60 to −100 mV from a holding potential of 40 mV) before and after (noted by *arrow*) application of 10 μM amiloride. As is clear in these representative experiments and summarized in Fig. 1*C*, isoleucine substitution of the conserved tryptophan and the residues just before and after were tolerated in α-mENaC. In contrast, tryptophan substitutions in β- and γ-mENaC were not tolerated resulting in non-active/functional channels. Notably, substitution of the critical tryptophan in α-mENaC, but not the residues just before and after, resulted in a significant reduction in ENaC activity. To test whether the effects of substitution resulted from improper expression of mutant subunits at the membrane, we quantified membrane expression using a standard membrane labeling strategy involving biotinylation of membrane proteins followed by streptavidin precipitation. Subunits of interest (mutants) were identified in Western blots of the membrane fraction and total cellular pools through an N-terminal Myc epitope tag. The results in the summary graph in Fig. 1*D* demonstrate that mutation has no effect on the relative membrane expression levels of mutant subunits *versus* wild-type subunits. Moreover, mutation also has no effect on total subunit expression levels.

As shown by the supplemental data in Fig. S1, we extended observations to other members of the ENaC/Deg channel superfamily by performing similar experiments on mutant rat ASIC containing alanine substitutions of the critical tryptophans conserved at the base of TM1 (ASIC1a^{W46A}, ASIC2b^{W45A}, and ASIC3^{W46A}). As demonstrated by the representative traces in supplemental Fig. S1*A* and summarized in supplemental Table S1B, substitution in rASIC resulted in loss of acid-evoked currents in voltage-clamped CHO cells expressing mutant homomeric channels. These results are consistent with the conserved transmembrane domain tryptophan serving an important functional role. Tolerance in α-ENaC at this site allowed further probing of the role played by this critical tryptophan.

The results in Fig. 2 demonstrate that it is the loss of the critical Trp rather than introduction of a novel amino acid, such as isoleucine, having distinct properties, that decreases activity. Fig. 2*A* shows summary results from voltage-clamp experiments quantifying ENaC activity for channels containing Phe, Ile, Gly, Lys, Glu, and Cys substitutions of Trp-112 in the α-subunit. Any replacement of Trp-112 significantly decreased activity. Surprisingly, the conserved substitution where aromatic Trp is replaced with aromatic Phe results in a statistically identical decrease in activity as the more invasive substitutions replacing Trp with large (Ile) and small (Gly) aliphatic residues, and a residue having a sulfur-containing side chain (Cys). Substitution with a polar residue was intolerable resulting in loss of function. Results in Fig. 2*B*, as those in Fig. 1*D*, demonstrate that these substitutions have no effect on the relative and total membrane levels of mutant α-mENaC subunits. Thus, whereas replacing Trp-112 in α-mENaC with any residue decreases activity, it appears that it is the actual loss of the critical tryptophan that is important for function rather than the characteristics of the newly introduced residue, with the caveat that polar

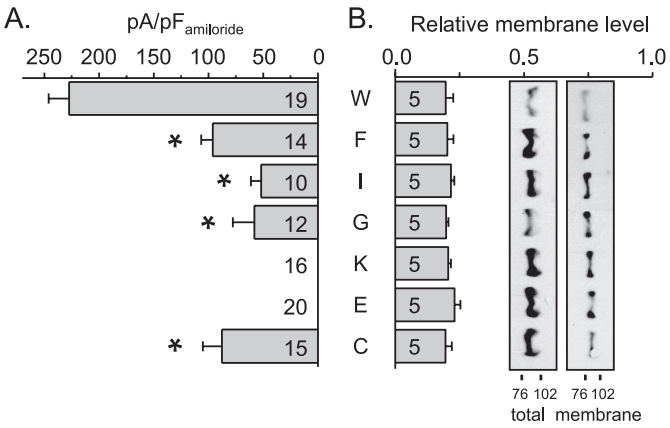

FIGURE 2. **Loss of the critical Trp at the base of TM1 causes decreases in activity.** *A*, summary graph of activity of wild-type channels and mutant channels containing α-mENaC with differential substitution of the critical Trp at the base of TM1. Identical to experiments in Fig. 1, the activity of recombinant ENaC was quantified as the amiloride-sensitive current density in voltage-clamped CHO cells. *, significant decrease compared with wild-type. *B*, summary graph of the relative membrane levels of the α-subunits in wild-type and mutant ENaC containing α-subunits with differentially substituted Trp. The *inset* shows representative Western blots: the *left* and *right* blots contain total cellular proteins and membrane fractions (4× concentrated), respectively. As in Fig. 1, blots are probed with anti-Myc antibody to identify α-subunits in wild-type and mutant channels.

residues have a profound impact, being particularly intolerable at this site.

Disruption of the Critical Trp in TM1 of α-ENaC Unmasks Voltage Sensitivity—We were surprised to observe that mutant channels containing α-subunits with Trp substitutions showed pronounced inward rectification compared with channels containing all wild-type subunits in macroscopic I-V curves generated in asymetrical solutions (raw currents shown in Fig. 1*B*, I-V curves not shown). Either a change in the single channel conductance or selectivity of mutant channels or a change in their (voltage dependence of) open probability could account for this response to voltage.

To test this further, we next compared the voltage dependence of activity of wild-type and mutant ENaC in voltage-clamped CHO cells in symmetrical NaCl solutions. Fig. 3*A* shows families of representative macroscopic currents evoked by test pulses ranging from 100 to −100 mV for wild-type channels and channels containing the W112C mutation. As expected at all voltages between 100 and −100 mV, instantaneous and steady-state currents were similar for wild-type channels with no noticeable time dependence of activation or voltage sensitivity. This is further highlighted by the I-V plots of instantaneous and steady-state macroscopic currents in Fig. 3*B* for wild-type and mutant ENaC. In contrast, channels containing mutant α-subunits had linear instantaneous currents similar to wild-type channels but larger relative inward steady-state currents at hyperpolarizing potentials and smaller outward steady-state currents at depolarizing potentials. Moreover, activation at hyperpolarizing potentials and deactivation at depolarizing potentials had significant time-dependent components. The G-V curve for steady-state current in Fig. 3*C* for channels containing W112C α-subunits emphasizes the voltage sensitivity of mutant channels. In contrast, the *inset* in Fig. 3*C* emphasizes that wild-type mENaC is not sensitive to voltage

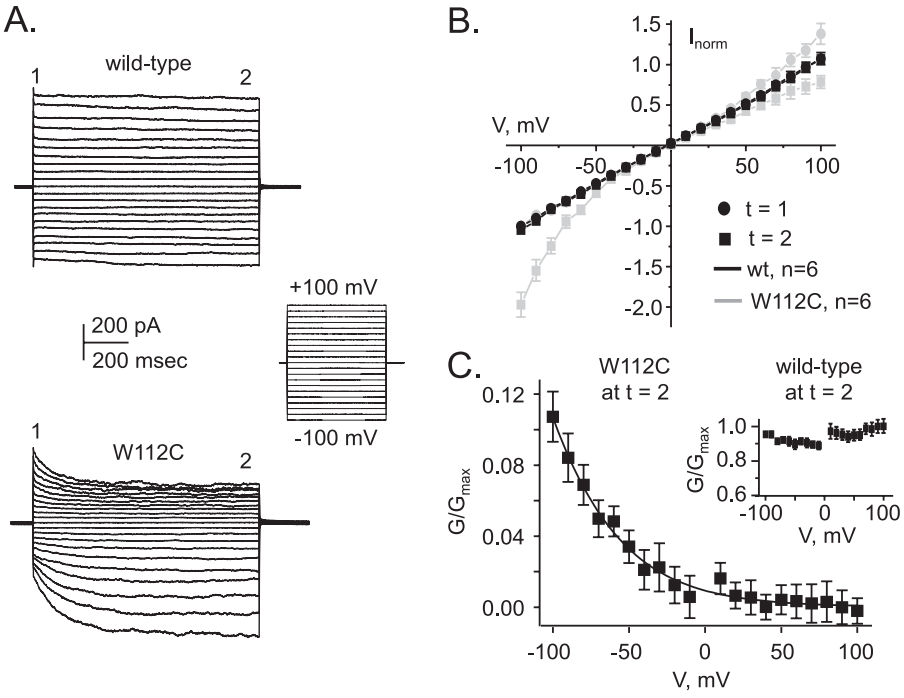

FIGURE 3. **ENaC containing α-subunits with substituted Trp sense voltage.** *A*, representative families of macroscopic currents evoked by a voltage-step protocol (shown to the *right*) for wild-type (*top*) and mutant ENaC (containing W112C α-subunits; *bottom*) in voltage-clamped CHO cells in symmetrical solutions. *B*, normalized macroscopic I-V relation for instantaneous ($t = 1$) and steady-state ($t = 2$) currents for wild-type and mutant ENaC from voltage-clamped CHO cells as in *A*. Currents normalized to instantaneous current at −100 mV. *C*, summary G-V curve showing the voltage dependence of steady-state currents from mutant ENaC. The *inset* shows wild-type. Data are collected from experiments similar to those described in *A*.

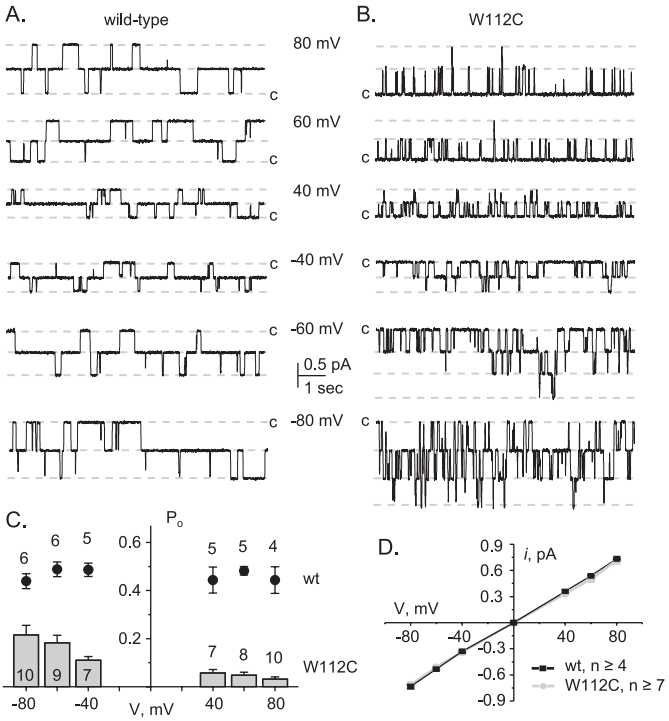

FIGURE 4. **Increases in P_o upon hyperpolarization underlie voltage sensitivity in mutant ENaC.** Representative single channel current traces at test potentials ranging from 80 to −80 mV in excised, outside-out patches for wild-type (*A*) and mutant ENaC (*B*, containing W112C α-subunits) expressed in CHO cells are shown. Experiments were performed in symmetrical LiCl solutions. Inward current is down. *C*, summary plot showing open probability as a function of test potential for wild-type and mutant ENaC. Data are from experiments similar to those described in *A* and *B*. *D*, summary *i*-V plots for wild-type and mutant ENaC from experiments similar to those described in *A* and *B*.

over this range. These results excluded a change in selectivity as underpinning voltage sensitivity in mutant ENaC, pointing to either a change in unitary conductance or open probability.

Voltage-dependent Changes in P_o Underlie the Voltage Sensitivity of Mutant ENaC—Fig. 4, *A* and *B*, respectively, show typical single channel current traces for wild-type channels and channels with W112C α-subunits in excised, outside-out patches in symmetrical 150 mM LiCl solutions at holding potentials ranging from 80 to −80 mV. As is clear in these representative traces and in the summary graph of P_o *versus* voltage shown in Fig. 4*C*, wild-type channels showed no voltage dependence of P_o over this voltage range. In contrast, there was a clear voltage-dependent change in P_o in mutant channels with P_o increasing as a function of hyperpolarization. Fig. 4*D* confirms that mutation has no effect on unitary current at any voltage: Unitary currents changed in a linear manner in response to voltage for wild-type and mutant channels. This is consistent with mutation not affecting unitary conductance or permeation with Li^+ permeating equally well from either direction. As expected, wild-type channels at all voltages had slow gating kinetics with open and closed times in the range of seconds. In contrast, there was a clear qualitative difference in the gating kinetics of mutant channels with open times (and possibly closed times) reduced particularly at depolarizing potentials. The low P_o of mutant channels prohibited detailed kinetic analysis for it was not always possible to establish the absolute number of mutant channels in these patches. This may have also led to overestimation of P_o for mutant channels; however, this does not affect conclusions of voltage sensitivity or about changes in P_o providing the underlying mechanism. These findings are in good agreement with those in Fig. 3 and support voltage-dependent changes in P_o as the mechanism underlying activation/deactivation and the voltage sensitivity of steady-state currents in mutant channels.

The Voltage Dependence of Activation and Deactivation for Mutant ENaC Are Similar—We quantified next the voltage dependence of activation and deactivation times for mutant ENaC from holding potentials of 80 and −80 mV, respectively. Fig. 5, *A* and *B*, show representative families of macroscopic currents evoked by hyperpolarizing and depolarizing test potentials, respectively, in voltage-clamped CHO cells expressing W112C mutant ENaC in symmetrical 150 mM NaCl. As summarized in Fig. 5*C*, both the tau of activation and deactivation changed in a linear manner in response to changes in voltage with hyperpolarization accelerating activation and

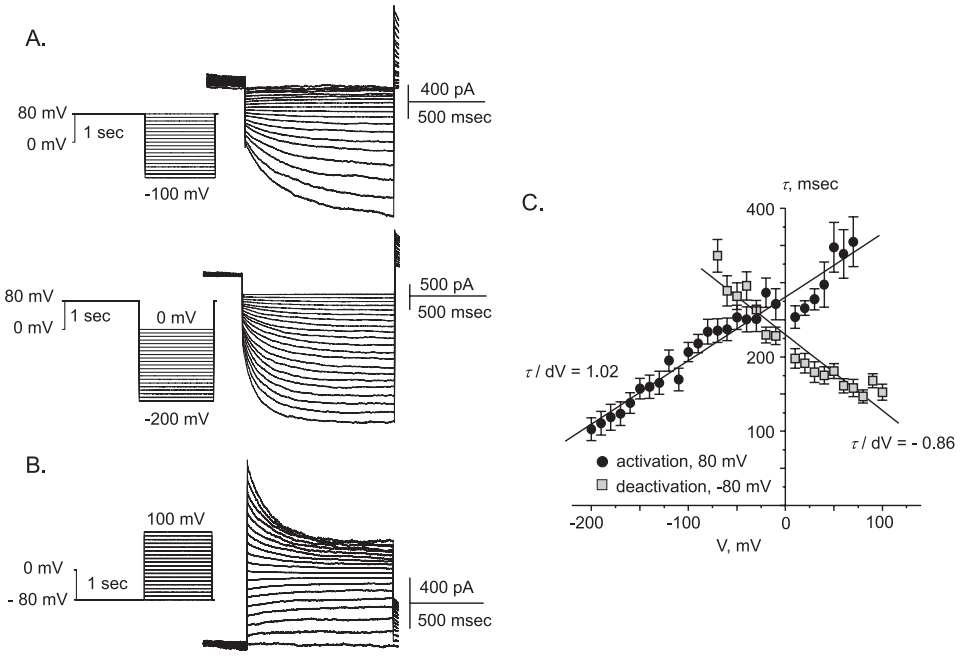

FIGURE 5. **The tau of activation and deactivation for mutant ENaC change in a linear manner as a function of voltage.** *A*, overlays of two representative families of macroscopic currents from mutant ENaC in a voltage-clamped CHO cell evoked by voltage protocols (shown to the *left*) built to quantify the tau of activation. Activation times were measured by stepping from the holding potential of 80 mV down to −100 mV (in 10-mV decrements) and from hold to −200 mV starting at 0 mV (in 10-mV decrements) with 1-s intervals at hold between each test potential. *B*, an overlay of a representative family of macroscopic currents from mutant ENaC in a voltage-clamped CHO cell evoked by a voltage protocol (shown to the *left*) built to quantify tau of deactivation. Deactivation times were measured by stepping to 100 mV (in 10-mV increments) from a holding potential of −80 mV with 1-s intervals at hold between each test potential. *C*, summary graph plotting $\tau_{activation}$ and $\tau_{deactivation}$ as a function of voltage. Data are from experiments similar to those described in *A* and *B*.

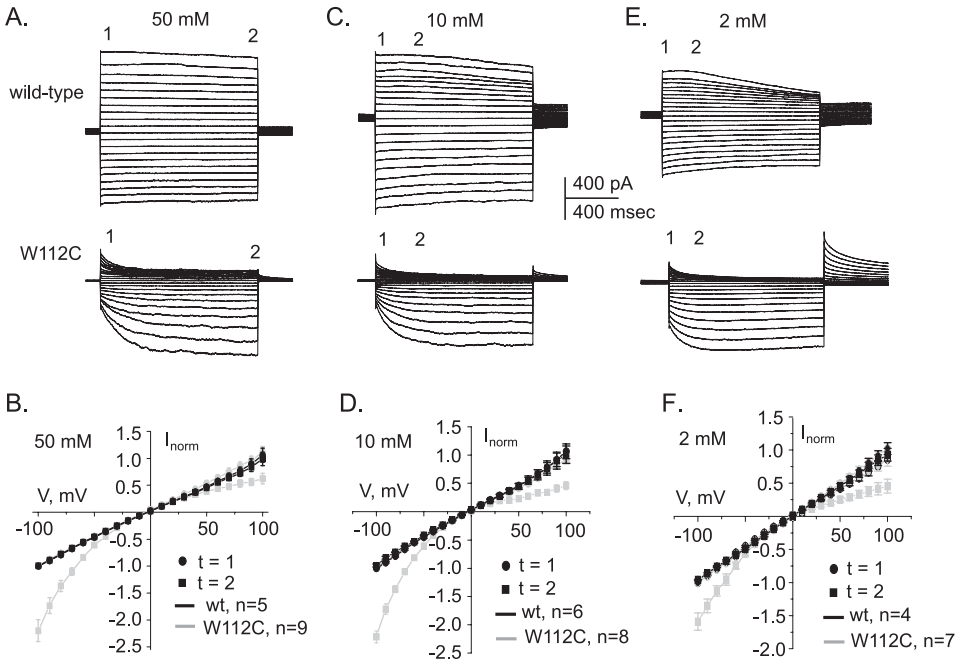

FIGURE 6. **I-V relation for mutant ENaC in symmetrical solutions with decreasing amounts of NaCl.** Representative families of macroscopic currents and summary I-V graphs for instantaneous and steady-state currents from voltage-clamped CHO cells expressing wild-type (*top*) and mutant (*bottom*) ENaC. Data were collected in symmetrical 50 (*A* and *B*), 10 (*C* and *D*), and 2 mM [Na^+] (*E* and *F*).

slowing deactivation; and depolarization slowing activation and accelerating deactivation. The absolute change in the tau of activation and deactivation as a function of voltage (τ/dV) was ~1.0 ms/mV.

Voltage Sensitivity of Mutant ENaC Is Independent of Divalent Cations but Dependent on [Na^+]—Because the voltage-dependent effects of ENaC mutation on open probability and the qualitative effect of mutation on single channel kinetics are reminiscent of an open channel block relieved by hyperpolarization (29, 30), we tested whether Ca^{2+} and Mg^{2+} affected voltage sensitivity. This was done by removing all divalent cations from our solutions and strongly buffering the remaining trace levels. Supplemental Fig. S2, *A* and *B* show representative macroscopic currents in a voltage-clamped CHO cell and summary I-V graph, respectively, for W112C channels in divalent cation-free solutions with symmetrical 150 mM Na^+. Macroscopic current through mutant ENaC in the absence of divalent cations was similar to that in their presence showing marked voltage-dependent activation and deactivation, and steady-state currents that increased with hyperpolarizing potentials.

The experiments above suggest that divalent cations have little role in the voltage sensitivity of mutant ENaC. Because ENaC is also sensitive to Na^+ (31–33), we wondered whether the absolute amount of Na^+ available to the channel would affect voltage sensitivity. To test this, we established I-V relations for wild-type and mutant ENaC expressed in CHO cells in voltage-clamp experiments with symmetrical NaCl solutions with decreasing amounts of [Na^+]. Fig. 6 shows representative macroscopic currents for wild-type and mutant ENaC and associated I-V curves for instantaneous and steady-state currents in the presence of 50 mM (*A* and *B*), 10 mM (*C* and *D*), and 2 mM (*E* and *F*) [Na^+]. Under all conditions and similar to that observed with symmetrical 150 mM [Na^+], hyperpolarization increased relative steady-state current and time-dependent activation and deactivation was notable for mutant channels. (As expected, prolonged depolarization and hyperpolarization in low [Na^+] ultimately disrupted gradients leading to a decrease in current at latter time points; thus, the steady-

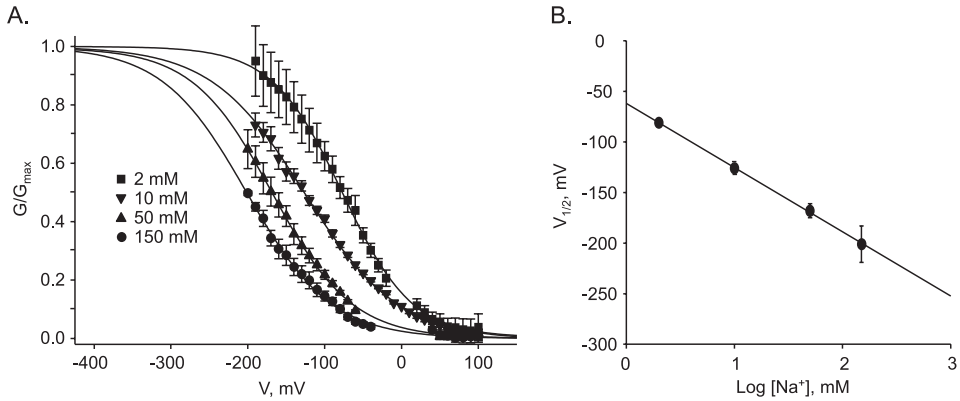

FIGURE 7. **Voltage sensitivity of mutant ENaC is [Na^+]-dependent.** *A*, summary G-V curves for steady-state currents from mutant ENaC acquired in symmetrical 150, 50, 10, and 2 mM [Na^+]. *B*, summary graph showing the voltage resulting in half-maximal activity at steady state, as established from G-V curves, for mutant ENaC as a function of Na^+ concentration.

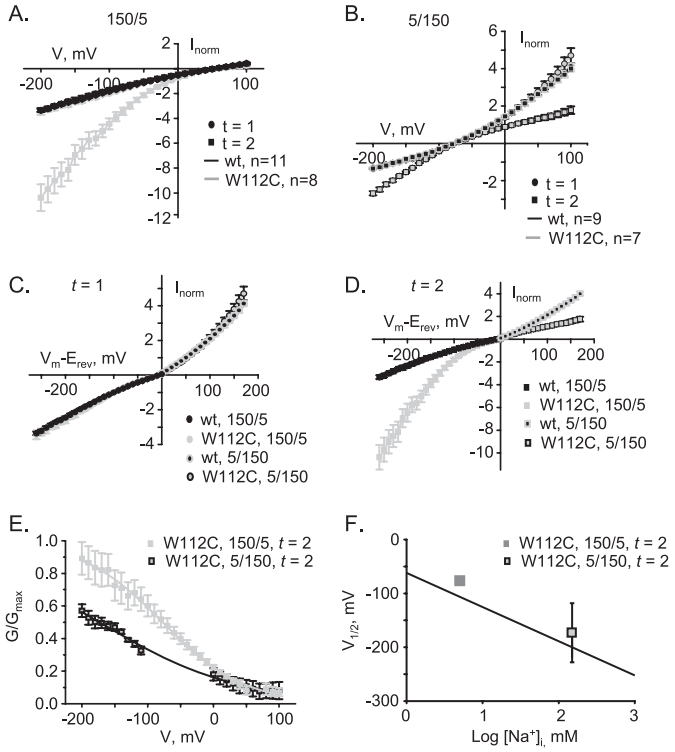

FIGURE 8. **Mutant ENaC is sensitive to intracellular [Na^+].** Current-voltage relations for instantaneous ($t = 1$) and steady-state ($t = 2$) macroscopic currents from wild-type and mutant (W112C) ENaC in voltage-clamped CHO cells in asymetrical (bath/pipette) 150/5 (*A*) and 5/150 (*B*) NaCl solutions. I-V relations for instantaneous (*C*) and steady-state (*D*) currents for wild-type and mutant ENaC corrected for reversal potential by subtracting E_{rev} from V_m and replotting the data with reversal through 0 mV. Inward currents were plotted from results with 150/5 gradients and outward currents from 5/150 gradients. *E*, G-V relation for steady-state currents from mutant ENaC in 150/5 and 5/150 solutions. *F*, summary graph showing the voltage resulting in half-maximal activity at steady state, as established from G-V curves, for mutant ENaC in asymetrical solutions as a function of intracellular [Na^+]. The curve for $V_{1/2}$ *versus* [Na^+] for mutant ENaC in symmetrical solutions from Fig. 7*B* is re-shown for comparison.

state current was quantified at $t = 400$ ms for 10 and 2 mM [Na^+].)

Fig. 7*A* shows steady-state G-V curves for W112C ENaC assessed in symmetrical 2, 10, 50, and 150 mM [Na^+]. As is clear in this summary figure, decreases in [Na^+] cause a marked rightward shift in the G-V curve of mutant ENaC. The [Na^+] dependence of this shift in the G-V curve is emphasized in Fig. 7*B* where the change in $V_{1/2}$ as a function of logarithmic [Na^+] is shown. For every 10-fold decrease in [Na^+], the voltage at which mutant ENaC was half-active increased by ~63 mV.

Mutant ENaC Is Sensitive to Intracellular [Na^+]—To distinguish between the actions of intracellular and extracellular [Na^+] on the voltage sensitivity of mutant ENaC, we explored the effects of asymetrical (solution bathing extracellular face/intracellular face of the channel) 150/5 and 5/150 mM Na^+ on the I-V and G-V relations of this channel. Fig. 8, *A* (150/5 Na^+) and *B* (5/150 Na^+) show summary I-V curves for instantaneous ($t = 1$) and steady-state ($t = 2$) currents for wild-type and mutant ENaC under asymetrical conditions. Instantaneous currents for both wild-type and mutant ENaC showed Goldmann rectification in asymetrical Na^+, as expected, for a channel highly selective for Na^+. Steady-state currents for wild-type channels were identical to instantaneous currents. This becomes clear upon re-plotting I-V relations (inward currents in 150/5 and outward currents in 5/150) as a function of voltage after correcting for differences in reversal potential because of asymetrical conditions ($V_m - E_{rev}$) as is done in Fig. 8, *C* and *D*. In contrast, relative steady-state currents for mutant channels under asymetrical conditions had decreased outward current (with 5/150) and increased inward current (with 150/5) compared with wild-type channels. Comparison of the G-V curves for mutant ENaC in these two asymetrical conditions, as shown in Fig. 8*E*, reveals sensitivity to intracellular Na^+: high relative intracellular [Na^+] shifts the curve to the left compared with low relative levels. Restating this, the G-V relation for mutant ENaC in the presence of 150 mM intracellular [Na^+] (and 5 mM extracellular [Na^+]) is similar to the G-V relation for this channel in symmetrical 150/150 [Na^+] solutions. Similarly, the G-V relation in the presence of 5 mM intracellular [Na^+] (and 150 mM extracellular [Na^+]) is closer to the G-V relation in symmetrical 2/2 [Na^+] solutions (see Fig. 7). As expected and shown in Fig. 8*F*, $V_{1/2}$ calculated from G-V relations for mutant ENaC in asymetrical solutions displayed as a function of intracellular [Na^+] closely parallels the line established in symmetrical solutions.

If voltage sensitivity is chiefly dependent on intracellular [Na^+], then eliminating intracellular sodium should abolish or lessen voltage dependence. This is exactly what happens. Fig. 9*A* shows representative single channel current traces for typical ENaC containing an W112C α-subunit in an excised, outside-out patch at voltages of 0 through −100 mV. For this experiment, asymetrical solutions were used where Na^+ was completely absent in the solution bathing the intracellular face of the channel. As is clear in this representative experiment and in the summary Fig. 9*B* of similar experiments, the absence of

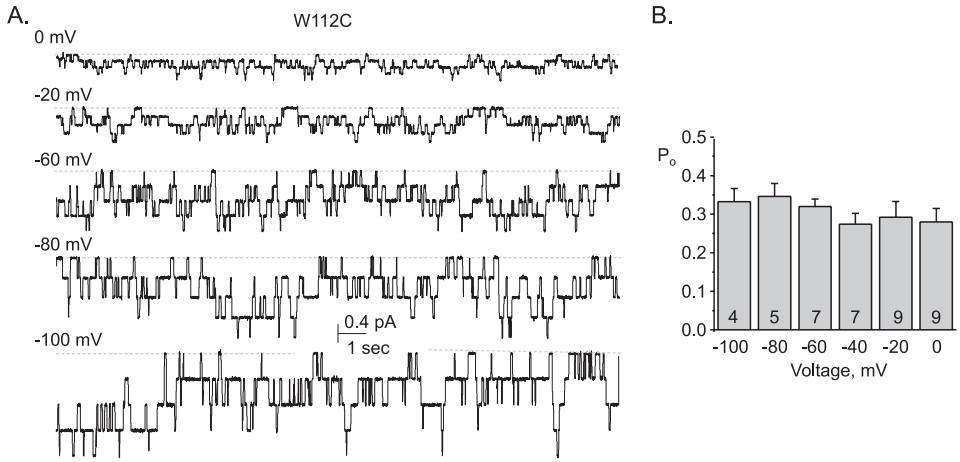

FIGURE 9. **Removal of intracellular Na^+ abolishes the voltage dependence of mutant ENaC.** *A*, representative single channel current traces at test potentials ranging from 0 to −100 mV in excised, outside-out patches for mutant ENaC containing W112C α-subunits expressed in CHO cells. Experiments performed in asymmetrical 150/0 NaCl solutions with no sodium in the solution bathing the intracellular face of the channel. Inward current is down. *B*, summary graph showing open probability as a function of test potential for mutant ENaC (assayed in outside-out patches) in asymetrical 150/0 NaCl. Data are from experiments similar to those described in *A*.

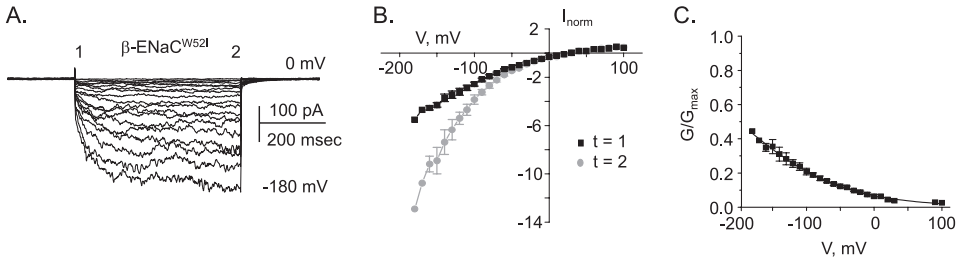

FIGURE 10. **Mutation of the critical Trp at the base of TM1 in β-ENaC also results in voltage sensitivity.** *A*, representative family of macroscopic currents from mutant ENaC (containing wild-type α- and γ-subunits and W52I-substituted β-subunits) in asymetrical 150/5 Na^+ solutions evoked by a voltage-step protocol in a voltage-clamped CHO cell. *B*, summary I-V curves for instantaneous and steady-state macroscopic currents from mutant ENaC containing W52I-substituted β-subunits. *C*, summary G-V curve for mutant ENaC containing the W52I β-subunit.

intracellular Na^+ dramatically lessened the voltage dependence of mutant ENaC.

The Trp at the Base of TM1 in β-mENaC Serves a Similar Function—After establishing the importance of intracellular Na^+ and voltage to regulation of mutant ENaC containing W112C α-subunits, we thought it important to revisit the apparently inactive/nonfunctional mutant ENaC containing Trp-substituted β- and γ-subunits. We retested the functionality of channels containing mutant β-subunits using recording conditions with low intracellular Na^+ and pronounced hyperpolarizing test pulses. With these more stringent conditions, channels containing wild-type α- and γ-ENaC and W52I-substituted β-subunits had small but measurable activity. Fig. 10 shows a representative family of macroscopic currents from W52I mutant ENaC ($n = 5$) in a voltage-clamped CHO cell. Similar to substitution of W112 in the α-subunit, the analogous substitution (Trp-52) in β-ENaC results in voltage sensitivity with notable activation times upon hyperpolarization. This becomes more apparent in the I-V and G-V curves shown for ENaC with mutant β-subunits in Fig. 10, *B* and *C*, respectively. Trp mutation in β-ENaC had a more profound effect on channel activity compared with mutation in α-ENaC, shifting the voltage dependence further left toward hyperpolarizing potentials. The voltage required to reach half-maximal activity for channels with mutant β-subunits is -200 ± 35 mV compared with -77 ± 4 mV for channels with mutant α-subunits (from Fig. 8) under identical (150/5 Na^+) conditions.

In contrast, strong hyperpolarization (to −200 mV) in the presence of low intracellular [Na^+] failed to elicit any activity for mutant channels containing Trp-substituted γ-subunits ($n = 27$; not shown). This suggests that either this mutation drastically shifts the $V_{1/2}$ to extreme hyperpolarizing voltages or that channels containing mutant γ-subunits are truly nonfunctional.

DISCUSSION

This is the first description of a mutation that enhances voltage sensitivity in ENaC. The voltage and Na^+ sensitivity of this mutant ENaC has many parallels with C-type inactivation of K^+ channels and pore block of NMDA receptors by Mg^{2+}. Thus, the mechanism underlying voltage-sensing in mutant ENaC may be related to these. Moreover, the position of the conserved Trp in ENaC at the base of TM1 at the membrane-cytosol interfacial region is similar to Trp residues in gramicidin A (gA) and KcsA channels and M_2 proton channels. Interfacial Trp residues in these ion channels serve distinct functions because of the position of their side chains.

Our finding that the conserved transmembrane domain Trp in ENaC is critical to protecting the channel from intracellular Na^+ and membrane voltage emphasizes the functional importance of this residue at this particular position. Our results argue that having Trp at the base of TM1 is an absolute requirement for normal ENaC/Deg channel activity. This likely arises from the unique properties Trp residues have at lipid-water interfaces in transmembrane domains.

The most surprising finding of the current study is the marked voltage sensitivity unmasked by Trp substitution. Rat ENaC has been reported to have intrinsic voltage sensitivity, where the P_o of channels with low resting activity increase upon hyperpolarization (31, 33–35). The magnitude of intrinsic voltage sensitivity of ENaC may be species-dependent. This is clear when considering the response of wild-type mENaC to voltage as presented in the current study.

The mechanism underlying intrinsic voltage sensitivity in rENaC is not fully understood but appears related to voltage-dependent changes in P_o with hyperpolarization shifting the channel from a low P_o state to a state with higher P_o (31, 34, 35).

This has many parallels with the voltage sensitivity noted in the current study for mENaC containing Trp mutants. Perhaps there is a relation here with Trp substitution in the current study enhancing an inherent voltage sensitivity in ENaC. If voltage sensitivity results from a spontaneous but graduated switching between different P_o states, then mutants having a more pronounced voltage sensitivity may have faster spontaneous transitions. The current finding that Trp substitution has no effect on single channel conductance, selectivity, and permeation but does affect P_o fits with this interpretation. Moreover, the fact that mutant ENaC at a macroscopic level has notable time components of activation in response to hyperpolarization and deactivation in response to depolarization may reflect a population of channels switching in a stochastic manner from lower to higher P_o states. If this is correct, then voltage influences the rate of change for mutant channels at a macroscopic level in a constant manner accelerating and decelerating spontaneous changes by ~1 ms/mV. Moreover, Trp at the base of TM1 must be protective in that it lessens the effects of voltage.

This raises questions about what causes voltage-dependent changes in P_o in mutant ENaC. The voltage sensitivity of this channel, which leads to inward rectification, as well as, the single channel characteristics are reminiscent of a reversible, voltage-sensitive pore block as typified by extracellular Mg^{2+} block of open NMDA receptors and block of K_{ir} channels by intracellular Mg^{2+} (29, 30). While we fail to observe any effect of divalent cations on voltage sensitivity of mutant ENaC, this concept fits nicely with the observations of others that ENaC activity is sensitive to intracellular Na^+ levels with increasing intracellular [Na^+] rapidly decreasing P_o (31, 33, 35). Rapid feedback regulation of ENaC is thought to be intrinsic to the channel likely resulting from direct effects of intracellular Na^+ on channel P_o.

Our observation that an increase in intracellular Na^+ causes a leftward shift in the G-V relation for mutant mENaC links voltage sensitivity and sensitivity to intracellular Na^+. In the context of pore block by a permeant ion, this link between voltage and Na^+ begins to make sense. The voltage sensitivity of ENaC may reflect inhibition by intracellular Na^+ with hyperpolarization relieving pore block by driving Na^+ out of the intracellular vestibule of the pore. This would not necessitate a change in conductance or perm-selectivity, but could appear as a voltage-dependent change in P_o as seen for Mg^{2+}, Na^+, and the polyamine block of K_{ir} and K_{ATP} channels, which leads to inward rectification of these latter channels (30, 36).

We note that the above interpretation is just one of several possible explanations for the results presented here, although, we believe it to be the best. Another feasible alternative that also fits is that there is an intracellular Na^+ binding site in the channel or a protein closely coupled to the channel that influences gating or gating state through an allosteric mechanism. Voltage would then affect either Na^+ binding to this site, or directly affect gating with allosteric modulation in response to Na^+ occupancy of the binding site. With the pore block scenario, voltage and Na^+ would not switch the channel between states with low and high open probability but rather switch the channel between states with increased and decreased probabilities of open channel block. We suspect this to be the case. Allosteric regulation, in contrast, would result in true transitions between states of low and high open probability.

Tryptophan residues are common to intrinsic membrane proteins at the limits of transmembrane domains at the lipid-water interface (20, 21). Here, they can act to anchor transmembrane domains, and through interactions with other residues form channel gates, depending on side chain orientation (16, 19, 37–40).

The side chains of the interfacial Trp at the ends of transmembrane domains of gA channel subunits run perpendicular to membrane lipids, parallel to the longitudinal axis of the lipid bilayer (16, 18). Here, they form stable hydrogen bonds with the phosphate oxygens in lipid head groups forming an external belt that runs around the outside of the mouth of the pore to provide stability. Disruption of these bonds changes the tilt of the transmembrane domain affecting hydrophobic mismatch with membrane lipids and interaction with pore-forming transmembrane domains both of which in turn influence channel function (16). The critical Trp at the base of TM1 in ENaC, if it has its side chains in a similar orientation, may provide a similar belt stabilizing how TM1 tilts across the membrane to pack against TM2 affecting pore properties including diameter and or placement of a gate. It is easy to conceive how substituting these Trp could lead to hydrophobic mismatch and/or affect TM1-TM2 interactions. Conceptually, this could unmask or augment an intrinsic pore block or allosteric mechanism causing mutant channels to become hypersensitive to voltage and Na^+. The stability provided to the channel, particularly the pore, by these anchoring Trp residues would allow it to function normally in protection against changes in intracellular Na^+ and membrane voltage.

In contrast to their orientation in gA channels, the side chains of interfacial tryptophans in M_2 proton channels project into the aqueous environment of the inner mouth of the pore (38, 40, 41). Here through interactions with other residues, these Trp form a ring-like structure inside the mouth of the pore akin to the bundle crossing of K^+ channels. Formation and disruption of this ring structure is involved in gating M_2 proton channels. If the side chains of Trp at the base of TM1 in ENaC/Deg channels project into the aqueous mouth of the pore, they may serve a similar function providing stability to the inner vestibule of the pore through the formation of an internal ring-like structure that prevents collapsing of the pore or functions as a gate.

Our studies establish an important link between regulation of ENaC by voltage and $[Na^+]_i$. Moreover, we establish here the critical importance to function of conserved Trp residues at the intracellular base of TM1 in ENaC/Deg channels: they mask intrinsic voltage and Na^+ sensitivity.

REFERENCES

1. Kellenberger, S., and Schild, L. (2002) *Physiol. Rev.* **82,** 735–767
2. Garty, H., and Palmer, L. G. (1997) *Physiol. Rev.* **77,** 359–396
3. Bianchi, L., and Driscoll, M. (2002) *Neuron* **34,** 337–340
4. Lifton, R. P., Gharavi, A. G., and Geller, D. S. (2001) *Cell* **104,** 545–556
5. Bonny, O., and Hummler, E. (2000) *Kidney Int.* **57,** 1313–1318
6. Jasti, J., Furukawa, H., Gonzales, E. B., and Gouaux, E. (2007) *Nature* **449,** 316–323

7. Staruschenko, A., Adams, E., Booth, R. E., and Stockand, J. D. (2005) *Biophys. J.* **88,** 3966–3975
8. Canessa, C. M., Schild, L., Buell, G., Thorens, B., Gautschi, I., Horisberger, J. D., and Rossier, B. C. (1994) *Nature* **367,** 463–467
9. Newbolt, A., Stoop, R., Virginio, C., Surprenant, A., North, R. A., Buell, G., and Rassendren, F. (1998) *J. Biol. Chem.* **273,** 15177–15182
10. Li, J., Sheng, S., Perry, C. J., and Kleyman, T. R. (2003) *J. Biol. Chem.* **278,** 13867–13874
11. Kellenberger, S., Hoffmann-Pochon, N., Gautschi, I., Schneeberger, E., and Schild, L. (1999) *J. Gen. Physiol* **114,** 13–30
12. Kellenberger, S., Auberson, M., Gautschi, I., Schneeberger, E., and Schild, L. (2001) *J. Gen. Physiol* **118,** 679–692
13. Kashlan, O. B., Maarouf, A. B., Kussius, C., Denshaw, R. M., Blumenthal, K. M., and Kleyman, T. R. (2006) *J. Biol. Chem.* **281,** 30455–30462
14. Pfister, Y., Gautschi, I., Takeda, A. N., van, Bemmelen, M., Kellenberger, S., and Schild, L. (2006) *J. Biol. Chem.* **281,** 11787–11791
15. Poët, M., Tauc, M., Lingueglia, E., Cance, P., Poujeol, P., Lazdunski, M., and Counillon, L. (2001) *EMBO J.* **20,** 5595–5602
16. Tang, P., and Xu, Y. (2002) *Proc. Natl. Acad. Sci. U.S.A.* **99,** 16035–16040
17. Ozdirekcan, S., Nyholm, T. K., Raja, M., Rijkers, D. T., Liskamp, R. M., and Killian, J. A. (2008) *Biophys. J.* **94,** 1315–1325
18. Haney, E. F., Lau, F., and Vogel, H. J. (2007) *Biochim. Biophys. Acta* **1768,** 2355–2364
19. Williamson, I. M., Alvis, S. J., East, J. M., and Lee, A. G. (2003) *Cell Mol. Life Sci.* **60,** 1581–1590
20. Yau, W. M., Wimley, W. C., Gawrisch, K., and White, S. H. (1998) *Biochemistry* **37,** 14713–14718
21. White, S. H., and Wimley, W. C. (1999) *Annu. Rev. Biophys. Biomol. Struct.* **28,** 319–365
22. Staruschenko, A., Dorofeeva, N. A., Bolshakov, K. V., and Stockand, J. D. (2007) *Dev. Neurobiol.* **67,** 97–107
23. Hesselager, M., Timmermann, D. B., and Ahring, P. K. (2004) *J. Biol. Chem.* **279,** 11006–11015
24. Pochynyuk, O., Staruschenko, A., Tong, Q., Medina, J., and Stockand, J. D. (2005) *J. Biol. Chem.* **280,** 37565–37571
25. Staruschenko, A., Patel, P., Tong, Q., Medina, J. L., and Stockand, J. D. (2004) *J. Biol. Chem.* **279,** 37771–37778
26. Tong, Q., Gamper, N., Medina, J. L., Shapiro, M. S., and Stockand, J. D. (2004) *J. Biol. Chem.* **279,** 22654–22663
27. Staruschenko, A., Nichols, A., Medina, J. L., Camacho, P., Zheleznova, N. N., and Stockand, J. D. (2004) *J. Biol. Chem.* **279,** 49989–49994
28. Booth, R. E., and Stockand, J. D. (2003) *Am. J. Physiol. Renal Physiol.* **284,** F938–F947
29. MacDonald, J. F., and Nowak, L. M. (1990) *Trends Pharmacol. Sci.* **11,** 167–172
30. Nichols, C. G., and Lopatin, A. N. (1997) *Annu. Rev. Physiol* **59,** 171–191
31. Palmer, L. G., and Frindt, G. (1988) *J. Gen. Physiol.* **92,** 121–138
32. Silver, R. B., Frindt, G., Windhager, E. E., and Palmer, L. G. (1993) *Am. J. Physiol.* **264,** F557–F564
33. Awayda, M. S. (1999) *Am. J. Physiol.* **277,** C216–C224
34. Ishikawa, T., Marunaka, Y., and Rotin, D. (1998) *J. Gen. Physiol* **111,** 825–846
35. Palmer, L. G., and Frindt, G. (1996) *J. Gen. Physiol.* **107,** 35–45
36. Loussouarn, G., Rose, T., and Nichols, C. G. (2002) *Trends Cardiovasc. Med.* **12,** 253–258
37. Witter, R., Nozirov, F., Sternberg, U., Cross, T. A., Ulrich, A. S., and Fu, R. (2008) *J. Am. Chem. Soc.* **130,** 918–924
38. Schnell, J. R., and Chou, J. J. (2008) *Nature* **451,** 591–595
39. Xiang, F., Cukier, R. I., and Bu, Y. (2007) *J. Phys. Chem. B* **111,** 12282–12293
40. Stouffer, A. L., Acharya, R., Salom, D., Levine, A. S., Di, Costanzo, L., Soto, C. S., Tereshko, V., Nanda, V., Stayrook, S., and DeGrado, W. F. (2008) *Nature* **451,** 596–599
41. Tang, Y., Zaitseva, F., Lamb, R. A., and Pinto, L. H. (2002) *J. Biol. Chem.* **277,** 39880–39886